Direct Implementation of High-Fidelity Three-Qubit Gates for Superconducting Processor with Tunable Couplers

Hao-Tian Liu,[1,2,*] Bing-Jie Chen,[1,2,*] Jia-Chi Zhang,[1,2] Yong-Xi Xiao,[1,2] Tian-Ming Li,[1,2] Kaixuan Huang,[3] Ziting Wang,[3] Hao Li,[3] Kui Zhao,[3] Yueshan Xu,[3] Cheng-Lin Deng,[1,2] Gui-Han Liang,[1,2] Zheng-He Liu,[1,2] Si-Yun Zhou,[1,2] Cai-Ping Fang,[1,2] Xiaohui Song,[1,2,4] Zhongcheng Xiang,[1,2,4] Dongning Zheng,[1,2,4] Yun-Hao Shi,[1,4,†] Kai Xu,[1,2,3,4,5,‡] and Heng Fan[1,2,3,4,5,§]

[1]*Beijing National Laboratory for Condensed Matter Physics, Institute of Physics, Chinese Academy of Sciences, Beijing 100190, China*

[2]*School of Physical Sciences, University of Chinese Academy of Sciences, Beijing 100049, China*

[3]*Beijing Key Laboratory of Fault-Tolerant Quantum Computing, Beijing Academy of Quantum Information Sciences, Beijing 100193, China*

[4]*Hefei National Laboratory, Hefei 230088, China*

[5]*Songshan Lake Materials Laboratory, Dongguan 523808, Guangdong, China*

(Received 2 February 2025; revised 9 April 2025; accepted 1 July 2025; published 29 July 2025)

Three-qubit gates can be constructed using combinations of single-qubit and two-qubit gates, making their independent realization unnecessary. However, direct implementation of three-qubit gates reduces the depth of quantum circuits, streamlines quantum programming, and facilitates efficient circuit optimization, thereby enhancing overall performance in quantum computation. In this work, we propose and experimentally demonstrate a high-fidelity scheme for implementing a three-qubit controlled-controlled-Z (CCZ) gate in a flip-chip superconducting quantum processor with tunable couplers. This direct CCZ gate is implemented by simultaneously leveraging two tunable couplers interspersed between three qubits to enable three-qubit interactions, achieving an average final state fidelity of 97.94% and a process fidelity of 93.54%. This high fidelity cannot be achieved through a simple combination of single- and two-qubit gate sequences from processors with similar performance levels. Our experiments also verify that multilayer direct implementation of the CCZ gate exhibits lower leakage compared to decomposed gate approaches. As a showcase, we utilize the CCZ gate as an oracle to implement the Grover search algorithm on three qubits, demonstrating high performance with the target probability amplitude significantly enhanced after two iterations. These results highlight the advantage of our approach, and facilitate the implementation of complex quantum circuits.

DOI: 10.1103/lvb9-pfr3

Typically, a universal set of quantum gates for computation requires only single-qubit and two-qubit gates, from which any multiqubit gate, such as three-qubit gates, can be composed. [1]. However, the direct construction and control of high-fidelity multiqubit gates remain crucial for advancing quantum computation [2], particularly, in achieving quantum error correction [3–5], quantum simulation [6], and scalable quantum algorithms in the noisy intermediate-scale quantum (NISQ) era [7]. The CCZ gate stands out as a pivotal three-qubit gate, enabling specific operations that are challenging to replicate using single- or two-qubit gates alone. This gate applies a phase shift only when all three qubits are in the target state, making it indispensable in applications like Grover's search algorithm [8,9] and quantum error correction codes [10–13]. Direct implementation of the CCZ gate can significantly reduce circuit complexity and depth, addressing the limitations associated with decomposing complex operations into sequences of simpler gates, which introduce cumulative errors and increase operational overhead.

Despite its significance, achieving a high-fidelity CCZ gate has proven challenging across various quantum platforms, including superconducting qubits [14–20], trapped ions [21,22], photonic systems [23], and cavity QED systems [24–27]. Previous attempts have often relied on synthesizing the three-qubit gate from sequences of controlled-NOT (CNOT) gates and single-qubit rotations [28–36], leading to complex gate sequences that extend operation times and introduce additional sources of error. Each additional gate in such sequences increases the likelihood of decoherence and operational errors, making direct implementation of the CCZ gate highly desirable for practical quantum computation. While previous works have demonstrated engineered three-body interactions through

*These authors contributed equally to this work.
†Contact author: yhshi@iphy.ac.cn
‡Contact author: kaixu@iphy.ac.cn
§Contact author: hfan@iphy.ac.cn

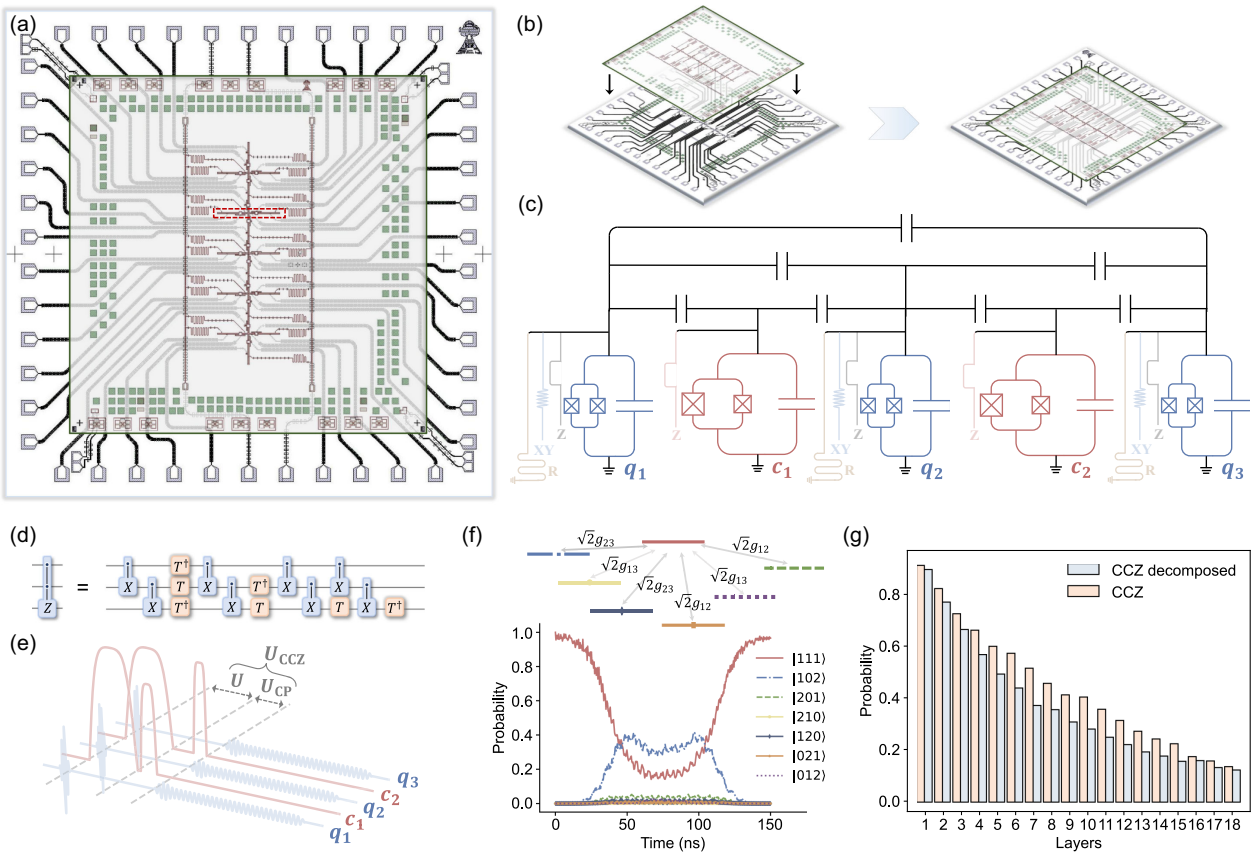

FIG. 1. (a) The flip-chip quantum processor with 21 superconducting qubits arranged in a 1D chain with multiple legs. Every two qubits are equipped with a coupler in between. (b) Schematic of flip-chip technique. (c) Circuit diagram of the implemented superconducting circuits framed by the red dotted line in (a), consisting of three qubits (q_1, q_2, q_3) and two couplers (c_1, c_2). The qubits have the independent XY and Z controls and readout resonators, while the couplers have only Z controls. (d) Quantum circuit of the CCZ gate decomposed into a series of single-qubit gates and CX (CNOT) gates. (e) Pulse sequence of the direct CCZ gate for superconducting qubits with tunable couplers. (f) Energy level diagram and time-dependent population transfer in the three-excitation manifold. (g) Comparison of multilayer leakage between the direct CCZ gate and its decomposed implementation.

purpose-designed superconducting circuits [37,38], these approaches often encounter inherent complexity and scalability challenges.

Experimental demonstrations of three-qubit gates in superconducting qubit systems have achieved a peak process fidelity of 98.26% [16]. However, to accommodate the continuously expanding scale, the state-of-the-art superconducting quantum chips employ flip-chip technology and tunable coupling architectures [39–41]. To realize high-fidelity and high-scalablity three-qubit gate operations on such multiqubit chips, we propose and experimentally demonstrate an optimized CCZ gate scheme using tunable couplers. Our approach leverages advanced fabrication techniques to directly implement high-fidelity three-qubit interactions while addressing common sources of error, such as residual two-qubit interactions and leakage to higher energy levels and couplers, through a targeted control sequence that minimizes nonadiabatic errors.

Our experiment is performed on a 21-qubit flip-chip quantum processor [Fig. 1(a)], where every two nearest-neighbor (NN) qubits are coupled through a tunable coupler. For the purposes of our investigation, we select a subset consisting of three qubits (q_1, q_2, q_3) and two interqubit couplers (c_1, c_2), as schematically shown in Fig. 1(c). The Hamiltonian of the total system is ($\hbar = 1$)

$$H = \sum_i \left(\omega_i b_i^\dagger b_i - \frac{\alpha_i}{2} b_i^\dagger b_i^\dagger b_i b_i\right) - \sum_{ij} g_{ij}(b_i - b_i^\dagger)(b_j - b_j^\dagger), \tag{1}$$

where b_i ($i \in \{1, 2, 3, c_1, c_2\}$) is the annihilation operator and g_{ij} denotes the direct capacitive coupling. Here all qubit frequencies and anharmonicities are fixed, i.e., $\omega_1/2\pi = 5.000$ GHz, $\omega_2/2\pi = 4.896$ GHz, $\omega_3/2\pi = 5.040$ GHz, $\alpha_1/2\pi = -198$ MHz, $\alpha_2/2\pi = -200$ MHz, $\alpha_3/2\pi = -206$ MHz, $\alpha_{c_1}/2\pi = -340$ MHz, and $\alpha_{c_2}/2\pi = -320$ MHz. By applying the Z pulses to the couplers, one can dynamically adjust the coupler frequencies to tune

the effective couplings between computational qubits. Recent approaches leverage this capability to implement high-fidelity controlled-Z (CZ) gates for superconducting qubits equipped with tunable couplers [42–50].

The routine method for preparing a CCZ gate involves combining a series of single-qubit gates and two-qubit CNOT gates [51], as illustrated in Fig. 1(d). In addition to implementing the CCZ gate using this conventional approach, we realize a direct CCZ gate with high scalability, which is composed of two segments [see Fig. 1(e)]. The first segment U is to achieve the accumulation of the controlled-controlled phase (CCPhase), in which the three qubits are unbiased but two couplers are simultaneously applied Z pulses to generating the three-qubit interaction. Here we set the pulses of these two couplers as flat-top Gaussian waveforms, parametrized by the same duration τ and the respective maximal amplitudes V_{c_1} and V_{c_2}. The calibration of pulse parameters primarily aims to optimize the CCPhase to $\pm\pi$ while minimizing leakage errors (specific calibration details will be described later). When the initial state is set to $|111\rangle$, the calibrated U induces the level repulsion between $|111\rangle$ and all other three-excitation states (e.g., $|102\rangle$ and $|201\rangle$), resulting in a pronounced effective three-body interaction. This engineered U dynamically suppresses leakage from the computational subspace by driving the population back toward $|111\rangle$ [Fig. 1(f)], while simultaneously introducing a three-qubit conditional phase. However, the first segment may also introduce two conditional phases (CPhases) of two pairs of NN qubits, namely q_1q_2 and q_2q_3. This occurs because changes in the coupler frequency can alter the effective ZZ interaction between the NN qubits connected to the coupler [42,52], leading to an accumulation of the CPhases over the duration τ. To compensate for these CPhases accumulated in the first segment, the second segment U_{CP} involves applying two-qubit CPhase gates sequentially to qubit pairs q_1q_2 and q_2q_3. The total length of the direct CCZ gate thus becomes $\tau + \tau_{12} + \tau_{23}$, where τ_{12} and τ_{23} represent the lengths of the respective CPhase gates. In the experiment, we take $\tau = 150$, $\tau_{12} = 62$, and $\tau_{23} = 44$ ns, yielding a total length for the direct CCZ gate of 256 ns. This is notably shorter than the typical total length of 640 ns achieved using the routine decomposition strategy. Consequently, the direct CCZ gate is expected to exhibit lower multilayer leakage due to decoherence, as demonstrated in Fig. 1(g).

In the following, we outline several key steps for calibrating the direct CCZ gate (see Fig. 2). The initial step (i) involves calibrating the individual qubits to ensure that they operate within optimal parameters at idle points. As required for subsequent steps, all single-qubit gates must be calibrated in advance at this stage. Furthermore, the calibration of the coupler Z distortion, including both short- and long-time distortion calibration [50], is essential for achieving high-fidelity two- and three-qubit gates. The second step (ii) focuses on identifying the optimal spot in the parameter space that yield the best performance for the CCZ gate. This includes optimizing the coupler Z pulse amplitudes V_{c_1} and V_{c_2} for a fixed $\tau = 150$ ns to achieve the desired $\pm\pi$ CCPhase while minimizing leakage errors. To measure the leakage, we prepare $|111\rangle$ by applying X gates to the three qubits and measure the population of $|111\rangle$ after U. To efficiently characterize the CCPhase, we initialize three qubits in six special states, i.e., $|0+0\rangle$, $|1+1\rangle$, $|1+0\rangle$, $|0+1\rangle$, $|10+\rangle$, and $|00+\rangle$. We then measure all conditional phases, i.e., $\varphi_{12} = \varphi_{|1+0\rangle} - \varphi_{|0+0\rangle}$, $\varphi_{23} = \varphi_{|0+1\rangle} - \varphi_{|0+0\rangle}$, $\varphi_{13} = \varphi_{|10+\rangle} - \varphi_{|00+\rangle}$, $\varphi_{123} = \varphi_{|1+1\rangle} - \varphi_{|0+0\rangle}$, where φ_{12}, φ_{23}, and φ_{13} represent the two-qubit conditional phases. Here φ_{123} is the three-qubit conditional phases when both control qubits q_1 and q_3 are excited to $|1\rangle$. It actually includes the CCPhase of CCZ and all the two-qubit conditional phases. Thus, the CCPhase of CCZ is given by $\varphi_{\mathrm{ccz}} = \varphi_{123} - \varphi_{13} - \varphi_{12} - \varphi_{23}$. As mentioned before, φ_{12} and φ_{23} can be compensated by applying corresponding CPhase gates. However, compensating for φ_{13} poses a significant challenge, as it necessitates a non-adjacent CPhase gate between q_1 and q_3. Although gate decomposition can be employed to achieve this, it may introduce additional complexity and noise, potentially degrading the overall fidelity of CCZ. Therefore, it is crucial to calibrate the system so that φ_{13} is as close to zero as possible, and thus $\varphi_{\mathrm{ccz}} \approx \varphi_{123} - \varphi_{12} - \varphi_{23}$. We try to search for an operating point where $\varphi_{\mathrm{ccz}} = \pm\pi$ while simultaneously minimizing the leakage and $|\varphi_{13}|$. As shown in Fig. 2(b), two relatively symmetrical optimal spots meet these criteria, indicated by the red circle and red star, respectively. Since the optimal spot marked by the star exhibits a smaller $|\varphi_{13}| \approx 0.0743$, we select it as our preferred operating point. These tune-up measurements are qualitatively reproduced by time-dependent Hamiltonian simulations for five interacting transmons with 3 levels [53]. Finally, we apply virtual Z gates [58] to compensate for the accumulations of single-qubit dynamic phases that accompany the CCZ gate. These dynamic phases can be first roughly characterized through Ramsey experiments on the three qubits, and then numerically optimized using the Nelder-Mead algorithm, with the quantum process tomography (QPT) χ-matrix fidelity serving as the objective function. In our QPT experiments, we construct a comprehensive set of 64 probe states by forming the tensor product of four single-qubit operations $\{I, X, X/2, Y/2\}$ for each of the three qubits ($4^3 = 64$). The resulting state fidelities and the χ-matrix after the calibration are shown in Fig. 2(c), where the average fidelity of these 64 states after (before) applying a CCZ gate is 97.06% (99.37%), and the process fidelity, calculated as $F_\chi = \mathrm{Tr}(\chi_{\mathrm{exp}}\chi_{\mathrm{ideal}})$, is 93.54%.

Under the assumption of negligible decoherence and no leakage to the environment, our numerical simulation of the direct CCZ gate, utilizing the time-dependent Hamiltonian, achieves an average state fidelity of 99.45% and a process

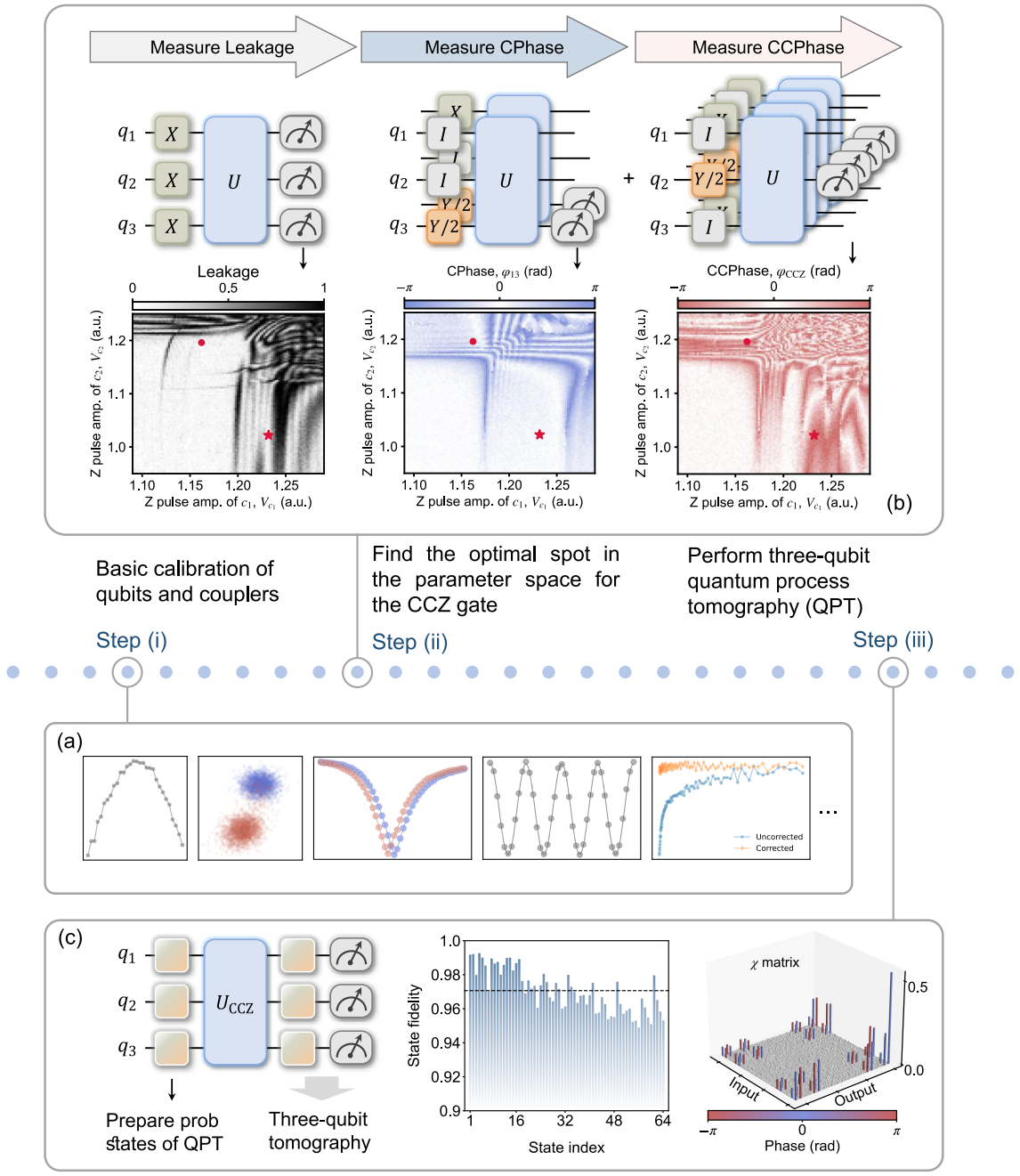

FIG. 2. Experimental measurements and calibrations for CCZ gate. (a) Basic calibration of qubits and couplers. (b) Calibration of the Z pulse amplitudes of couplers for the CCZ gate. The optimal operating points, where $\varphi_{ccz} = \pm\pi$ while both leakage and φ_{13} approach zero, are marked by a dot and a star. Given that the working point marked by the star has a smaller $|\varphi_{13}|$, we select it as the preferred operating point. The circuits to measure leakage, CPhase, and CCPhase are illustrated at the middle. (c) Experimental data of quantum process tomography (QPT) of the CCZ gate. From left to right are the QPT circuit, the fidelities of 64 prob states, and χ matrix. The average final state fidelity is 97.06% and the process fidelity is 93.54%.

fidelity of 98.75%. These high fidelities underscore the exceptional potential of our proposed scheme. However, the observed discrepancies between the simulation and experimental results are mainly attributed to the influence of decoherence (see Supplemental Material [53] for details). As experimental technology advances and the quality of quantum devices improves, it is anticipated that these discrepancies will diminish, further enhancing the performance of the three-qubit gates on large-scale quantum chips.

To demonstrate the performance of the CCZ gate, we first plot the truth table for computational basis states in

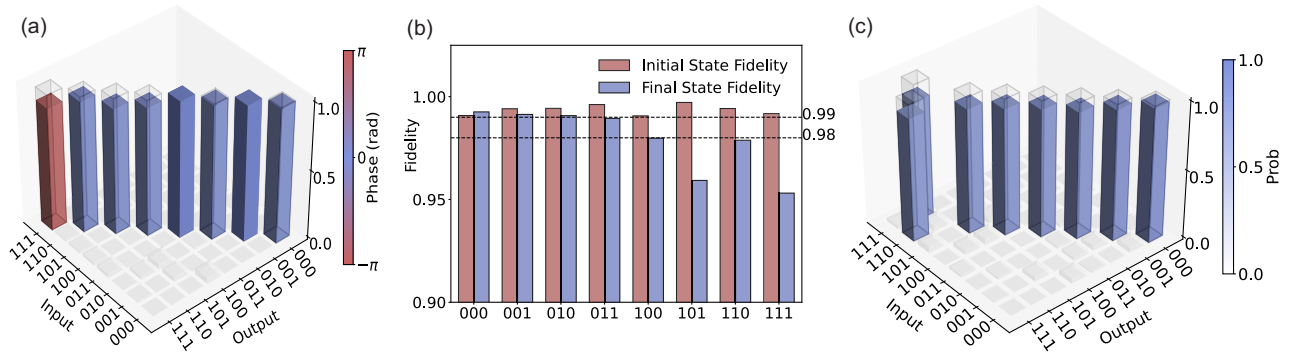

FIG. 3. Experimental results for the CCZ and Toffoli gates. (a) The truth table of the CCZ gate. Theoretical probabilities are represented by transparent cylinders, while experimental probabilities and conditional phases are depicted by the height and color of solid cylinders, respectively. The average fidelity of the truth table is 96.52%. (b) The state fidelity of the CCZ gate. The average final state fidelity is 97.94%. (c) The truth table of the Toffoli gate. Theoretical probabilities appear as hollow cylinders, with experimental probabilities indicated by the color bar.

Fig. 3(a). The visibility of the measured truth table is $\mathrm{Tr}[U_{\mathrm{exp}}U_{\mathrm{ideal}}]/8 = 96.52\%$, with an average final state fidelity of 97.94% [Fig. 3(b)], indicating high accuracy and precision in our measurements. Furthermore, by combining the CCZ gate with Hadamard gates, we construct a Toffoli (CCNOT) gate. As shown in Fig. 3(c), the corresponding truth table exhibits a visibility of 92.83%, underscoring the versatility and effectiveness of our CCZ gate implementation for advanced multiqubit operations.

In addition, we utilize the calibrated CCZ gate to demonstrate an example of the three-qubit Grover search algorithm (GA) [8,59]. As a fundamental quantum algorithm, GA leverages quantum coherence as a resource to speed up the process of searching for a target state. It requires the system to be initialized to the maximum superposition state $|\psi_0\rangle$ and repeated by the Grover operator $G = DO$, where $O = 1\text{–}2|s\rangle\langle s|$ ($|s\rangle$ is the target state) serves as the oracle and $D = 2|\psi_0\rangle\langle\psi_0| - 1$ is diffusion operator, performing an inversion about average operation. The general principle of GA is briefly shown in Fig. 4(a). In this demonstration, we initialize the qubits with three Hadamard gates to create a superposition of all possible states. We then use the CCZ gate as the oracle to mark the target state $|s\rangle = |111\rangle$. To implement the diffusion operator, we combine the CCZ gate with three Hadamard gates and three X gates, as depicted in Fig. 4(b). Theoretically, GA searches for the target state $|111\rangle$ among eight computational states. The optimal number of iterations is given by $\pi/4\sqrt{1/N} \approx 2.22$ [2], where $N = 8$ denotes the search space size. Our experimental results closely align with theoretical predictions, i.e., the probability amplitude of the target state is significantly higher than that of other states after two Grover iterations, as illustrated in Fig. 4(c). This result demonstrates the effective implementation of the GA using our CCZ gate.

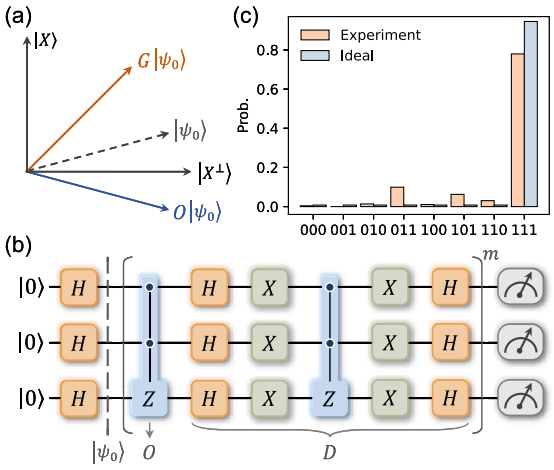

FIG. 4. Demonstration of three-qubit Grover search algorithm. (a) Schematic diagram of Grover algorithm principle. (b) Quantum circuit of three-qubit Grover search algorithm. (c) Probability data after two Grover operations.

In conclusion, we propose a high-fidelity scheme for implementing a three-qubit CCZ gate in superconducting quantum devices. Our method achieves an average state fidelity of 97.94% and a process fidelity of 93.54%, demonstrating its high performance. This method is scalable and requires minimal connectivity between qubits and couplers, offering significant advantages in terms of gate length and leakage compared to the decomposed CCZ gate schemes. We further validate the efficacy of our approach by successfully utilizing the CCZ gate to construct the Toffoli gate and implement the Grover search algorithm. Numerical simulations reveal that our proposed method for implementing the CCZ gate can theoretically attain an average state fidelity of 99.45% and a process fidelity of 98.75%, underscoring the outstanding potential of our scheme. Our work is expected to substantially contribute to the advancement of complex quantum algorithms and the realization of scalable quantum systems by providing a reliable and high-fidelity multiqubit gate operation.

Acknowledgments—This work was supported by the National Natural Science Foundation of China (Grants No. T2121001, No. 92265207, No. T2322030, No. 12122504, No. 12274142, No. 92365206, No. 12104055, No. 12204528, No. 92365301, and No. 12404578), the Innovation Program for Quantum Science and Technology (Grant No. 2021ZD0301800), Beijing National Laboratory for Condensed Matter Physics (2024BNLCMPKF022), the Beijing Nova Program (No. 20220484121), and the China Postdoctoral Science Foundation (Grant No. GZB20240815). This work was supported by the Synergetic Extreme Condition User Facility (SECUF). Devices were made at the Nanofabrication Facilities at Institute of Physics, CAS in Beijing.

Data availability—The data that support the findings of this article are openly available [60].

[1] A. Barenco, C. H. Bennett, R. Cleve, D. P. DiVincenzo, N. Margolus, P. Shor, T. Sleator, J. A. Smolin, and H. Weinfurter, Elementary gates for quantum computation, Phys. Rev. A **52**, 3457 (1995).
[2] M. A. Nielsen and I. L. Chuang, *Quantum Computation and Quantum Information* (Cambridge University Press, Cambridge, England, 2000).
[3] A. Y. Kitaev, Quantum computations: Algorithms and error correction, Russ. Math. Surv. **52**, 1191 (1997).
[4] T. Itoko, M. Malekakhlagh, N. Kanazawa, and M. Takita, Three-qubit parity gate via simultaneous cross-resonance drives, Phys. Rev. Appl. **21**, 034018 (2024).
[5] D. Bluvstein *et al.*, Logical quantum processor based on reconfigurable atom arrays, Nature (London) **626**, 58 (2024).
[6] L. B. Nguyen, Y. Kim, A. Hashim, N. Goss, B. Marinelli, B. Bhandari, D. Das, R. K. Naik, J. M. Kreikebaum, A. N. Jordan, D. I. Santiago, and I. Siddiqi, Programmable Heisenberg interactions between Floquet qubits, Nat. Phys. **20**, 240 (2024).
[7] J. Preskill, Quantum computing in the NISQ era and beyond, Quantum **2**, 79 (2018).
[8] L. K. Grover, Quantum mechanics helps in searching for a needle in a haystack, Phys. Rev. Lett. **79**, 325 (1997).
[9] T. Roy, S. Hazra, S. Kundu, M. Chand, M. P. Patankar, and R. Vijay, Programmable superconducting processor with native three-qubit gates, Phys. Rev. Appl. **14**, 014072 (2020).
[10] M. D. Reed, L. DiCarlo, S. E. Nigg, L. Sun, L. Frunzio, S. M. Girvin, and R. J. Schoelkopf, Realization of three-qubit quantum error correction with superconducting circuits, Nature (London) **482**, 382 (2012).
[11] A. Paetznick and B. W. Reichardt, Universal fault-tolerant quantum computation with only transversal gates and error correction, Phys. Rev. Lett. **111**, 090505 (2013).
[12] T. J. Yoder, R. Takagi, and I. L. Chuang, Universal fault-tolerant gates on concatenated stabilizer codes, Phys. Rev. X **6**, 031039 (2016).
[13] S. E. Rasmussen, K. Groenland, R. Gerritsma, K. Schoutens, and N. T. Zinner, Single-step implementation of high-fidelity *n*-bit Toffoli gates, Phys. Rev. A **101**, 022308 (2020).
[14] A. J. Baker, G. B. P. Huber, N. J. Glaser, F. Roy, I. Tsitsilin, S. Filipp, and M. J. Hartmann, Single shot i-Toffoli gate in dispersively coupled superconducting qubits, Appl. Phys. Lett. **120**, 054002 (2022).
[15] T. Bækkegaard, L. B. Kristensen, N. J. S. Loft, C. K. Andersen, D. Petrosyan, and N. T. Zinner, Realization of efficient quantum gates with a superconducting qubit-qutrit circuit, Sci. Rep. **9**, 13389 (2019).
[16] Y. Kim, A. Morvan, L. B. Nguyen, R. K. Naik, C. Jünger, L. Chen, J. M. Kreikebaum, D. I. Santiago, and I. Siddiqi, High-fidelity three-qubit iToffoli gate for fixed-frequency superconducting qubits, Nat. Phys. **18**, 783 (2022).
[17] C. W. Warren, J. Fernández-Pendás, S. Ahmed, T. Abad, A. Bengtsson, J. Biznárová, K. Debnath, X. Gu, C. Križan, A. Osman, A. F. Roudsari, P. Delsing, G. Johansson, A. F. Kockum, G. Tancredi, and J. Bylander, Extensive characterization and implementation of a family of three-qubit gates at the coherence limit, npj Quantum Inf. **9**, 44 (2023).
[18] L. B. Nguyen, N. Goss, K. Siva, Y. Kim, E. Younis, B. Qing, A. Hashim, D. I. Santiago, and I. Siddiqi, Empowering a qudit-based quantum processor by traversing the dual bosonic ladder, Nat. Commun. **15**, 7117 (2024).
[19] N. J. Glaser, F. Roy, and S. Filipp, Controlled-controlled-phase gates for superconducting qubits mediated by a shared tunable coupler, Phys. Rev. Appl. **19**, 044001 (2023).
[20] C. Song, S.-B. Zheng, P. Zhang, K. Xu, L. Zhang, Q. Guo, W. Liu, D. Xu, H. Deng, K. Huang, D. Zheng, X. Zhu, and H. Wang, Continuous-variable geometric phase and its manipulation for quantum computation in a superconducting circuit, Nat. Commun. **8**, 1061 (2017).
[21] B.-L. Fang, Z. Yang, and L. Ye, Scheme for implementing an n-qubit controlled not gate with superconducting quantum interference devices in cavity qed, Int. J. Quantum. Inform. **08**, 1337 (2010).
[22] T. Monz, K. Kim, W. Hänsel, M. Riebe, A. Villar, P. Schindler, M. Chwalla, M. Hennrich, and R. Blatt, Realization of the quantum Toffoli gate with trapped ions, Phys. Rev. Lett. **102**, 040501 (2009).
[23] Q. Wang, D. Lyu, J. Liu, and J. Wang, Polarization and orbital angular momentum encoded quantum Toffoli gate enabled by diffractive neural networks, Phys. Rev. Lett. **133**, 140601 (2024).
[24] C.-Y. Chen, M. Feng, and K.-L. Gao, Toffoli gate originating from a single resonant interaction with cavity QED, Phys. Rev. A **73**, 064304 (2006).
[25] H.-M. Shi, Y.-F. Yu, and Z.-M. Zhang, Three-qubit quantum-gate operation with an SQUID in a cavity, Chin. Phys. B **21**, 064205 (2012).
[26] A. Joshi and M. Xiao, Three-qubit quantum-gate operation in a cavity QED system, Phys. Rev. A **74**, 052318 (2006).
[27] J. K. Moqadam, R. Portugal, N. F. Svaiter, and G. d. O. Corrêa, Analyzing the Toffoli gate in disordered circuit QED, Phys. Rev. A **87**, 042324 (2013).
[28] H. Wei, Y. Di, and Y. Wang, Synthesis of some three-qubit gates and their implementation in a three spins system coupled with Ising interaction, Sci. China Phys. Mech. Astron. **53**, 664 (2010).

[29] L. Banchi, N. Pancotti, and S. Bose, Quantum gate learning in qubit networks: Toffoli gate without time-dependent control, npj Quantum Inf. **2**, 16019 (2016).
[30] M. J. Gullans and J. R. Petta, Protocol for a resonantly driven three-qubit Toffoli gate with silicon spin qubits, Phys. Rev. B **100**, 085419 (2019).
[31] S. P. Pedersen, K. S. Christensen, and N. T. Zinner, Native three-body interaction in superconducting circuits, Phys. Rev. Res. **1**, 033123 (2019).
[32] S. Daraeizadeh, S. P. Premaratne, N. Khammassi, X. Song, M. Perkowski, and A. Y. Matsuura, Machine-learning-based three-qubit gate design for the Toffoli gate and parity check in transmon systems, Phys. Rev. A **102**, 012601 (2020).
[33] S.-N. Sun, B. Marinelli, J. M. Koh, Y. Kim, L. B. Nguyen, L. Chen, J. M. Kreikebaum, D. I. Santiago, I. Siddiqi, and A. J. Minnich, Quantum computation of frequency-domain molecular response properties using a three-qubit iToffoli gate, npj Quantum Inf. **10**, 55 (2024).
[34] N. Yu, R. Duan, and M. Ying, Five two-qubit gates are necessary for implementing the Toffoli gate, Phys. Rev. A **88**, 010304(R) (2013).
[35] D. Maslov, Advantages of using relative-phase Toffoli gates with an application to multiple control Toffoli optimization, Phys. Rev. A **93**, 022311 (2016).
[36] X. Gu, J. Fernández-Pendás, P. Vikstål, T. Abad, C. Warren, A. Bengtsson, G. Tancredi, V. Shumeiko, J. Bylander, G. Johansson, and A. F. Kockum, Fast multiqubit gates through simultaneous two-qubit gates, PRX Quantum **2**, 040348 (2021).
[37] T. Menke, W. P. Banner, T. R. Bergamaschi, A. Di Paolo, A. Vepsäläinen, S. J. Weber, R. Winik, A. Melville, B. M. Niedzielski, D. Rosenberg, K. Serniak, M. E. Schwartz, J. L. Yoder, A. Aspuru-Guzik, S. Gustavsson, J. A. Grover, C. F. Hirjibehedin, A. J. Kerman, and W. D. Oliver, Demonstration of tunable three-body interactions between superconducting qubits, Phys. Rev. Lett. **129**, 220501 (2022).
[38] M. T. P. Nguyen, M. Rimbach-Russ, L. M. K. Vandersypen, and S. Bosco, Single-step high-fidelity three-qubit gates by anisotropic chiral interactions, arXiv:2503.12182.
[39] F. Arute *et al.*, Quantum supremacy using a programmable superconducting processor, Nature (London) **574**, 505 (2019).
[40] R. Acharya *et al.*, Suppressing quantum errors by scaling a surface code logical qubit, Nature (London) **614**, 676 (2023).
[41] R. Acharya *et al.*, Quantum error correction below the surface code threshold, Nature (London) **638**, 920 (2024).
[42] M. C. Collodo, J. Herrmann, N. Lacroix, C. K. Andersen, A. Remm, S. Lazar, J.-C. Besse, T. Walter, A. Wallraff, and C. Eichler, Implementation of conditional phase gates based on tunable ZZ interactions, Phys. Rev. Lett. **125**, 240502 (2020).
[43] Y. Xu, J. Chu, J. Yuan, J. Qiu, Y. Zhou, L. Zhang, X. Tan, Y. Yu, S. Liu, J. Li, F. Yan, and D. Yu, High-fidelity, high-scalability two-qubit gate scheme for superconducting qubits, Phys. Rev. Lett. **125**, 240503 (2020).
[44] H. Xu, W. Liu, Z. Li, J. Han, J. Zhang, K. Linghu, Y. Li, M. Chen, Z. Yang, J. Wang, T. Ma, G. Xue, Y. Jin, and H. Yu, Realization of adiabatic and diabatic CZ gates in superconducting qubits coupled with a tunable coupler, Chin. Phys. B **30**, 044212 (2021).
[45] Y. Ye *et al.*, Realization of high-fidelity controlled-phase gates in extensible superconducting qubits design with a tunable coupler, Chin. Phys. Lett. **38**, 100301 (2021).
[46] L. Ding, M. Hays, Y. Sung, B. Kannan, J. An, A. Di Paolo, A. H. Karamlou, T. M. Hazard, K. Azar, D. K. Kim, B. M. Niedzielski, A. Melville, M. E. Schwartz, J. L. Yoder, T. P. Orlando, S. Gustavsson, J. A. Grover, K. Serniak, and W. D. Oliver, High-fidelity, frequency-flexible two-qubit fluxonium gates with a transmon coupler, Phys. Rev. X **13**, 031035 (2023).
[47] R. Barends *et al.*, Diabatic gates for frequency-tunable superconducting qubits, Phys. Rev. Lett. **123**, 210501 (2019).
[48] Y. Sung, L. Ding, J. Braumüller, A. Vepsäläinen, B. Kannan, M. Kjaergaard, A. Greene, G. O. Samach, C. McNally, D. Kim, A. Melville, B. M. Niedzielski, M. E. Schwartz, J. L. Yoder, T. P. Orlando, S. Gustavsson, and W. D. Oliver, Realization of high-fidelity CZ and ZZ-free iSWAP gates with a tunable coupler, Phys. Rev. X **11**, 021058 (2021).
[49] I. N. Moskalenko, I. A. Simakov, N. N. Abramov, A. A. Grigorev, D. O. Moskalev, A. A. Pishchimova, N. S. Smirnov, E. V. Zikiy, I. A. Rodionov, and I. S. Besedin, High fidelity two-qubit gates on fluxoniums using a tunable coupler, npj Quantum Inf. **8**, 130 (2022).
[50] T.-M. Li *et al.*, High-precision pulse calibration of tunable couplers for high-fidelity two-qubit gates in superconducting quantum processors, Phys. Rev. Appl. **23**, 024059 (2025).
[51] P. M. Q. Cruz and B. Murta, Shallow unitary decompositions of quantum Fredkin and Toffoli gates for connectivity-aware equivalent circuit averaging, APL Quantum **1**, 016105 (2024).
[52] X. Li, T. Cai, H. Yan, Z. Wang, X. Pan, Y. Ma, W. Cai, J. Han, Z. Hua, X. Han, Y. Wu, H. Zhang, H. Wang, Y. Song, L. Duan, and L. Sun, Tunable coupler for realizing a controlled-phase gate with dynamically decoupled regime in a superconducting circuit, Phys. Rev. Appl. **14**, 024070 (2020).
[53] See Supplemental Material at http://link.aps.org/supplemental/10.1103/lvb9-pfr3, which includes Refs. [14,54–57], for additional information on the experimental setup, the principle of the gate, and detailed discussions of the numerical simulations.
[54] P. Zhao, D. Lan, P. Xu, G. Xue, M. Blank, X. Tan, H. Yu, and Y. Yu, Suppression of static *ZZ* interaction in an all-transmon quantum processor, Phys. Rev. Appl. **16**, 024037 (2021).
[55] S. P. Fors, J. Fernández-Pendás, and A. F. Kockum, Comprehensive explanation of ZZ coupling in superconducting qubits, arXiv:2408.15402.
[56] T. Abad, J. Fernández-Pendás, A. Frisk Kockum, and G. Johansson, Universal fidelity reduction of quantum operations from weak dissipation, Phys. Rev. Lett. **129**, 150504 (2022).
[57] T. Abad, A. F. Kockum, and G. Johansson, Impact of decoherence on the fidelity of quantum gates leaving the computational subspace, Quantum **9**, 1684 (2025).

[58] D. C. McKay, C. J. Wood, S. Sheldon, J. M. Chow, and J. M. Gambetta, Efficient Z gates for quantum computing, Phys. Rev. A **96**, 022330 (2017).

[59] C. Figgatt, D. Maslov, K. A. Landsman, N. M. Linke, S. Debnath, and C. Monroe, Complete 3-Qubit Grover search on a programmable quantum computer, Nat. Commun. **8**, 1918 (2017).

[60] H.-T. Liu *et al.*, Data for "Direct Implementation of High-Fidelity Three-Qubit Gates for Superconducting Processor with Tunable Couplers", 10.5281/zenodo.15792648 (2025).